arXiv:0904.4381v2 [astro-ph.CO] 12 Nov 2009

Density profile, velocity anisotropy and line-of-sight mass contamination of SLACS gravitational lenses

Antonio C. C. Guimarães and Laerte Sodré Jr.
Departamento de Astronomia, Universidade de São Paulo,
Rua do Matão 1226,CEP 05508-090 São Paulo - SP, Brazil
aguimaraes@astro.iag.usp.br

ABSTRACT

Data from 58 strong lensing events surveyed by the Sloan Lens ACS Survey is used to estimate the projected galaxy mass inside their Einstein radii by two independent methods: stellar dynamics and strong gravitational lensing. We perform a joint analysis of these two estimates inside a model with three degrees of freedom with respect to the lens density profile, stellar velocity anisotropy and a possible line-of-sigh (l.o.s.) mass contamination. We also consider two possibilities for the lens light distribution (Jaffe and Hernquist profiles). A Bayesian analysis is employed to estimate the model parameters, evaluate their significance and compare models. We find that the data favor Jaffe's profile over Hernquist's, but that any particular choice between these two does not change the qualitative conclusions with respect to the features of the system that we investigate. The data do not strongly constrain the l.o.s. mass contamination, yielding no contribution from secondary matter at maximum likelihood and an average contamination of the order of 10%, when considering the full range of probabilities. The density profile is compatible with an isothermal, being sightly steeper and having an uncertainty in the logarithmic slope of the order of 5%. We identify a degeneracy between the density profile slope and the anisotropy parameter, but we encounter no evidence in favor of an anisotropic velocity distribution on average for the whole sample.

Subject headings: dark matter — galaxies: elliptical and lenticular, cD — galaxies: kinematics and dynamics — galaxies: structure — galaxies: fundamental parameters — gravitational lensing

1. Introduction

The observation of strong gravitational lensing events has allowed many studies about the mass, density profile and structure of the galaxies that act as lenses (Bolton et al. 2006; Treu et al. 2006; Koopmans et al. 2006; Gavazzi et al. 2007; Bolton et al. 2007, 2008a,b; Czoske et al. 2008; Treu et al. 2008), which could also have important implications for dark matter and cosmology studies – see also Kochanek's contribution in Meylan et al. (2006) for a more general review in the field. Therefore it is fundamental to control for possible systematic effects, such as line-of-sight (l.o.s.) mass contamination. However most of these works consider a free path from source to lens and from lens to observer, even though there are observational and theoretical suggestions that the l.o.s. mass contamination may be significant.

Bar-Kana (1996) investigated theoretically the effect of the Large-Scale Structure on strong lensing events, finding that it can be significant. Keeton et al. (1997) observed that external shear due to galaxies and clusters associated with the primary lens or along the l.o.s. can be an important perturbation in individual lens models. Premadi & Martel (2004) used ray-tracing to investigate the effect of density inhomogeneities along the l.o.s. of strong lenses and concluded that it can be of order 10% on the magnification of the sources. Dalal et al. (2005) found that significant errors can arise from l.o.s. pro-

jections when using giant arcs generated by cluster strong lensing to constrain the cosmological parameters. Wambsganss et al. (2005) noted that secondary matter along the l.o.s. of strong lenses can lead in some circumstances to an overestimate of 10-15% of the primary lens mass if ignored. Using spectroscopy, various groups (Tonry & Kochanek 2000; Momcheva et al. 2006; Fassnacht et al. 2006; Williams et al. 2006; Auger et al. 2007) discovered a significant l.o.s. effect on strong lens galaxies. Moustakas et al. (2007) observed that even in under-dense local environments, the l.o.s. contamination may give a considerable contribution to galaxy-scale strong lenses. Using ray-tracing thought the Millennium Simulation, Hilbert et al. (2007) determined that strong lensing lines-of-sight are biased towards higher than average mean densities, contributing a few percent to the total surface density, and Puchwein & Hilbert (2009) found that secondary matter along the l.o.s. has a large effect on the strong-lensing optical depth and the cross-section for cluster strong lensing. Treu et al. (2008) measured the over-density of galaxies around SLACS lenses and observed that typical contributions from external mass distributions are of order of few percent, but reaching 10-20% in some cases. Faure et al. (2008) considered strong and weak lensing observations in the COSMOS survey and compared with simulations, finding that strong lensed images with large angular separation were in the densest regions. On the other hand, Auger (2008) did not find an over-density of photometric sources along the l.o.s. of a limited sample of SLACS strong lenses in comparison with other SDSS massive early-type galaxies and interpreted that as evidence against a possible l.o.s. contamination.

In this paper we use two independent galaxy mass estimate methods, strong gravitational lensing and stellar dynamics, to examine the presence of l.o.s. mass contamination in the lens set and its effect on the determination of the density profile. We use all the suitable events in the SLACS sample, considering realistic brightness functions for the lens-galaxies, and incorporating our prior ignorance on their velocity anisotropy.

In Section 2 we describe how we calculate the mass of SLACS lenses using strong gravitational lensing and stellar dynamics, and how we determine the l.o.s. mass contamination. In Section 3 we show our results, which are discussed in Section 4, together with our conclusions.

2. Data and Methods

The analysis in this paper is based on the comparison of galaxy masses calculated through two different methods: gravitational lensing and dynamical analysis. In sec. 2.1 we present the data used in the analysis, collected from the SLACS survey.

In sections 2.2 and 2.3, we discuss the lensing and dynamical mass determinations, respectively. We will assume simple models for the galaxy mass distribution (e.g., spherical symmetry, power-law density distribution) because they have few free parameters and allow to illustrate well the two methods. For a similar approach see Koopmans et al. (2006).

We want to examine whether the two mass estimates are indeed equivalent and/or if there is evidence of systematic differences between them. In particular, we consider the plausibility of a contamination affecting the lensing mass. Sec. 2.4 presents a Bayesian analysis of this problem.

2.1. Data

The selected set of galaxies is part of the Sloan Lens ACS Survey, SLACS (Bolton et al. 2006), which is a Hubble Space Telescope (HST) Snapshot imaging survey for strong gravitational galactic lenses. The candidates for the HST imaging were selected spectroscopically from the SDSS database and are a sub-sample of the SDSS Luminous Red Galaxy (LRG) sample.

We use data compiled from Koopmans et al. (2006), Gavazzi et al. (2007) and Bolton et al. (2008a), constructing a sample of 58 strong gravitational lensing events where the lenses are isolated early-type galaxies (E+S0). Data from SLACS is especially suitable for joint strong lensing and dynamical analysis because they allow precise determination (5% error) of the Einstein radius for each lens-galaxy in a relatively homogeneous sample of early-type galaxies. And, at the same time, SDSS has precise stellar velocity dispersion measurements (6% average error) for the lenses, as well as redshifts for lenses and background sources.

For each lens system we are interested in the redshift of the background lensed source z_s, the redshift of the lens z_l, the average stellar velocity dispersion inside an aperture σ_{ap}, the effective angular radius θ_{ef} and the Einstein angular radius θ_E. The sample average values for these quantities are $\langle z_l \rangle = 0.2$, $\langle z_s \rangle = 0.6$, $\langle \sigma_{ap} \rangle = 250 kms^{-1}$, $\langle \theta_{ef} \rangle = 2.2''$, and $\langle \theta_E \rangle = 1.2''$.

The source and lens redshifts were determined from the SDSS spectra, and the stellar velocity dispersion corresponds to the light-weighted average inside the $3''$ diameter SDSS fiber.

2.2. Lensing Mass

The estimated projected mass inside the Einstein radius $R_E = \theta_E D_L$, is given by

$$M_L = \frac{c^2}{4G} \frac{D_L D_S}{D_{LS}} \theta_E^2 \, , \tag{1}$$

where $D_{[L,S,LS]}$ is the angular-diameter distance of the lens, source, and between lens and source, respectively. These distances are calculated assuming a redshift-distance relation derived inside a chosen cosmological model that in the present paper is a concordance ΛCDM model with $\Omega_m = 0.3$, $\Omega_\Lambda = 0.7$ and $h = 0.7$.

The Einstein radii were determined from HST images using strong lensing modeling of the lenses and reconstruction of the unlensed sources (Koopmans et al. 2006; Gavazzi et al. 2007). The uncertainties on θ_E were reported to be around 5%, so we use this value for all Einstein radii when calculating the error on M_L. Note that the lensing modeling uses a Singular Isothermal Ellipsoid (SIE) mass model, but the resulting projected mass distribution is parameterized by an Eintein radius so that the enclosed mass in the projected ellipse is the same that would be enclosed in a projected circle from an equivalent Singular Isothermal Sphere. This is the radius we adopt here. Indeed, the Einstein radius determined this way is a robust attribute of the lens, being little sensitive to the lens model used [see Kochanek's contribution in Meylan et al. (2006)].

2.3. Dynamical Mass

We call the dynamical mass, m_D, the mass estimated from the observed velocity dispersion. Here we are interested in examining the case of a power law for the density profile, $\rho = Ar^\gamma$, where A is a constant that has to be determined from the Jeans equation and the observed velocity dispersion. The mass within the cylinder C_E of Einstein radius R_E is then

$$m_D(\gamma, \beta) = \int_{C_E} \rho(r) dV = \frac{2\pi^{3/2}}{3+\gamma} \frac{\Gamma\left(-\frac{1+\gamma}{2}\right)}{\Gamma\left(-\frac{\gamma}{2}\right)} A R_E^{3+\gamma}. \tag{2}$$

The spherical Jeans equation (Binney & Tremaine 1987) can be written as

$$\frac{1}{\nu} \frac{d(\nu\sigma_r^2)}{dr} + 2\frac{\beta\sigma_r^2}{r} = -\frac{d\Phi}{dr} = -\frac{\pi G}{3+\gamma} A r^{1+\gamma}, \tag{3}$$

where σ_r is the radial velocity dispersion, $\nu(r)$ is the luminosity density profile (Jaffe 1983; Hernquist 1990), $\beta \equiv 1 - \sigma_t^2/\sigma_r^2$ is the anisotropy parameter of the velocity distribution (σ_t is the tangential velocity dispersion), and Φ is the gravitational potential produced by the assumed density profile.

Since what is available is the luminosity-weighted average velocity dispersion within a given aperture, σ_{ap}^2, the following constraint is necessary for the determination of the constant A:

$$\sigma_{ap}^2 = \frac{\int_{C_{ap}} \nu\sigma_r^2 dV}{\int_{C_{ap}} \nu dV} \, , \tag{4}$$

where the integration volume is an infinite cylinder of radius R_{ap} with axis along the l.o.s.

To simplify, and since there is very little prior knowledge on the velocity anisotropy parameter, we assume that β is a constant. In Appendix A.1 we give more details on the solution of the Jean's equation (3), and in Appendix A.2 we examine the correction due to seeing effects.

Figure 1 displays the general behavior of the dynamical mass as a function of the density profile slope and velocity anisotropy parameter. We examine $m_D(\gamma, \beta = 0)$ and $m_D(\gamma = -2, \beta)$. Other combinations around these fixed values give qualitatively similar results. The doted line depicts the strong lensing mass for this hypothetical system, so it is possible to glimpse from the intersection of the curves the expected value of the dynamical parameters, γ and β. The difference of the curves calculated using the Jaffe or the Hernquist light profiles are just quantitative. The use of a constant mass to light ratio, $\nu(r) \propto \rho(r) \propto r^\gamma$, displayed as the dot-dashed line on the left panel of

figure 1, gives a very distinct and interesting behavior for $m_D(\gamma)$, reproducing a result obtained by Guimarães & Sodré (2007). However, a single power law is not a realistic approximation for the light distribution of the lens-galaxies in the sample.

2.4. Statistical Model

We want to compare the estimates of lensing and dynamical masses taking into account the possibility that masses obtained through gravitational lensing are affected by some type of contamination. Specifically, we consider a model where the real lensing mass m_L (assumed equal to the dynamical mass) is related to the measured lensing mass by

$$m_L(f_c) = (1 - f_c)M_L \ , \tag{5}$$

where f_c gives the fractional mass contamination.

Our model, then, has three free parameters: f_c, γ and β. These parameters are determined through the Bayes theorem. Since, however, we shall assume uniform priors for the parameters (see below), the posterior probability of the parameters is equivalent to the likelihood.

To construct a likelihood for the system, which has the mission of describing the probabilities of the model parameters given the data, we define the quantity

$$F = \frac{m_L}{m_D} - \frac{m_D}{m_L}. \tag{6}$$

Note that both m_L and m_D refer to the projected mass withing the Einstein radius. The likelihood for each lens system is then written as

$$\mathcal{L}_i = \frac{1}{\sqrt{2\pi}\sigma_{F,i}^2} \exp\left[-\frac{(F_t - F_{obs,i})^2}{2\sigma_{F,i}^2}\right], \tag{7}$$

where $F_{obs} = F_{obs}(f_c, \gamma, \beta; data)$ is the measured F given the model and the observational data, and F_t is the expected value for it, which, in the desired case where both m_L and m_D are estimates of the same true galaxy mass, corresponds to $F_t = 0$. Note that other quantities may be defined to construct the likelihood, for example $F = m_L/m_D + m_D/m_L$ ($F_t = 2$), $F = m_L/m_D$ ($F_t = 1$), $F = m_L - m_D$ ($F_t = 0$). The next to last definition gives a likelihood that is not symmetrical between m_L and m_D, what is not desirable, and the last example has the inconvenience of maximizing the likelihood not only in the desired region of the parameter space in which $m_L \sim m_D$, but also in the region where both mass estimates are small, what introduces artificial solutions that give maximum l.o.s. contamination. However if $f_c = 0$ is fixed, then all definitions for F, including the last, give very similar results.

The variance in F is estimated as being (an index i is implied in all quantities)

$$\sigma_F^2 = \frac{\left(m_L^2 + m_D^2\right)^2}{m_L^4 m_D^4}\left(m_L^2\sigma_D^2 + m_D^2\sigma_L^2\right), \tag{8}$$

where $\sigma_{\{D,L\}}$ is the uncertainty in $m_{\{D,L\}}$.

The joint likelihood for the whole set of N galaxies is then given by

$$\mathcal{L}(f_c, \gamma, \beta) = \prod_{i=1}^{N} \mathcal{L}_i, \tag{9}$$

which allows us to find the maximum likelihood estimator for the free parameters that we denote by putting a hat over the parameter ($\hat{f}_c$, $\hat{\gamma}$, $\hat{\beta}$), and the Bayes estimator (also called the posterior mean) defined by (all priors used are flat)

$$\langle p \rangle \equiv \frac{\int \mathcal{L}(p) p dp}{\int \mathcal{L}(p) dp}. \tag{10}$$

We also calculate the root mean square deviation, $\mathrm{rms}(p) = \sqrt{\langle p^2 \rangle - \langle p \rangle^2}$, for each free parameter and the Bayesian evidence (Trotta 2008)

$$E \equiv \int \mathcal{L}(p) P(p) dp \ , \tag{11}$$

where $P(p)$ is the prior probability distribution in the parameter space p. We adopt a flat prior probability distribution for all the parameters considered: $f_c \in [0, 0.5]$, $\gamma \in [-3, -1]$ and $\beta \in [-1, 1]$. We sample the parameter space using a grid and use it to make the various calculations.

The main appeal of this approach for model comparison is that the Bayesian evidence automatically implements Occam's razor by penalizing more strongly more complex models, those with more free parameters.

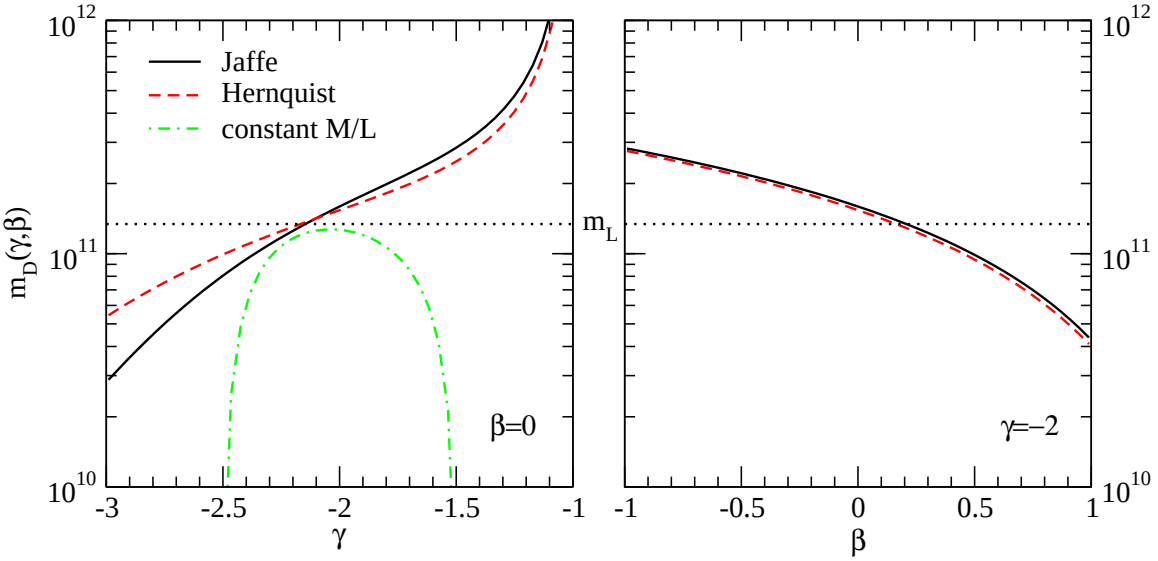

Fig. 1.— Dynamical mass behavior in relation to density profile logarithmic slope, γ, and the velocity anisotropy parameter, β, in units of $h^{-1}M_{\odot}$. The curves were calculated for an "average" system with $z_l = 0.2$, $z_s = 0.6$, $\sigma_{ap} = 250 kms^{-1}$, $\theta_E = 1.2''$, $\theta_{ef} = 2.2''$. Solid lines use Jaffe and dashed use Hernquist light distribution profiles. The dotted line depicts the strong lensing mass, equation (1), for the "average" system: $M_L = 1.34 \cdot 10^{11} h^{-1} M_{\odot}$. The dot-dashed line on the left panel was obtained using $\nu(r) \propto \rho(r) \propto r^{\gamma}$.

3. Results

We have analyzed the data described in Section 2.1 with a model with three degrees of freedom, one (f_c) corresponding to a possible l.o.s. mass contamination that would affect the strong lensing estimate of the lens mass and two (γ and β) corresponding to intrinsic properties of the lens that determine its dynamical mass estimate. Two light distribution profiles (Jaffe and Hernquist) were examined.

Table 1 summarizes the results for the maximum likelihood and Bayes estimators for each free parameter, as well as for their root mean square deviations, which give a measure of their dispersion. For the fractional mass contamination the maximum likelihood estimator is zero (no l.o.s. contamination), but its mean value is of the order of 10%. The density profile logarithmic slope is estimated to be close to an isothermal profile, using the Jaffe's light distribution, or somewhat steeper, using Hernquist's. In both cases it is found a $\sim 5\%$ dispersion, what is considerably higher than what was found by Koopmans et al. (2009) ($\sim 1\%$), neglecting l.o.s. contamination and anisotropy. The overall effective velocity anisotropy parameter is compatible with the null value (isotropy). We note that Koopmans et al. (2009) found a positive anisotropy (significantly distinct from isotropy) for the same sample, but using for that an independent determination based on scaling relations of the density profile logarithmic slope. That is a different method from ours, which relies solely on the joint strong lensing and dynamical analysis.

Figure 2 shows the likelihood marginalizations over one free parameter. The top row plots use Jaffe's profile and the bottom ones, Hernquist's. In figure 3 the marginalizations are over two free parameters. Qualitatively, the results for both profiles are the same. The likelihood distribution for the fractional mass contamination indicates a peak in $f_c = 0$ with a tail falling to $f_c \sim 0.5$ in the 3σ confidence region.

For γ and β the likelihood follows a near Gaussian behavior, their maximum likelihood and mean values are about the same. Jaffe's light distribution implies a slightly flatter density profile and higher anisotropy compared to Hernquist's. The f_c marginalized likelihoods (last row of figure 2) show a degeneracy between γ and β that was

Table 1: Maximum likelihood parameters, posterior means and root mean squares.

light profile	$\hat{f_c}$	$\langle f_c \rangle$	rms(f_c)	$\hat{\gamma}$	$\langle \gamma \rangle$	rms(γ)	$\hat{\beta}$	$\langle \beta \rangle$	rms(β)
Jaffe	0.	0.13	0.11	-2.04	-2.08	0.12	0.11	0.20	0.21
Hernquist	0.	0.10	0.09	-2.18	-2.13	0.11	-0.01	0.05	0.17

already hinted in figure 1, since the curves for $m_D(\gamma, \beta = 0)$ and $m_D(\gamma = -2, \beta)$ have monotonically crescent and decrescent behavior, respectively.

If the l.o.s. contamination is neglected, fixing $f_c = 0$ in our model, there is no significant change in the determination of the density profile logarithmic slope. However if the velocity distribution is assumed to be isotropic ($\beta = 0$), then there is a small steepening of the density profile, $\hat{\gamma} = -2.12$, and the probability distribution dispersion is smaller, rms(γ) = 0.06 when using Jaffe's light profile, compared with the model with three degrees of freedom (Table 1). Similarly, for Hernquist's profile, there is no significant change in $\hat{\gamma}$ and rms(γ) = 0.07.

If both fractional contamination and anisotropy are fixed, $f_c = \beta = 0$, then $\hat{\gamma} = 0.12$ for both light profiles and rms(γ) = 0.019 using Jaffe and rms(γ) = 0.027 using Hernquist. Therefore, the neglect of our ignorance on β and, to a lower extent, f_c, by fixing them equal to zero, implies a considerable underestimate of the dispersion in γ and possibly the introduction of a systematical error. In the central panel of figure 3 it is shown the likelihood (narrower curves) for a model with fixed $f_c = \beta = 0$, free γ and Hernquist profile, reproducing closely what was obtained by Koopmans et al. (2009). In the same figure we examine the impact of the seeing correction (see Appendix A.2). The two narrow and very close curves differ just in that in their calculation one takes into account the seeing correction (dot-dashed line) and the other (dotted line) does not. The seeing correction is negligible.

To compare models we calculate the ratio of the Bayesian evidences, also known as Bayes factor,

$$B(M_1, M_2) = \frac{E(M_1)}{E(M_2)}, \qquad (12)$$

which values can be interpreted qualitatively using Jeffrey's scale (Trotta 2008).

Table 2 gives a summary of several model comparisons. The Bayes factor between the models using Jaffe's or Hernquist's light profile indicates that the first is favored over the second. We also compare the gain in Bayesian evidence yielded by each free parameter separately in relation to a model with fixed values ($f_c = 0$, $\gamma = -2$, $\beta = 0$). In general, there is no or weak evidence favoring the simpler models (with fixed parameter values) over the more complex ones. However, if all parameter values are fixed the resulting model with no free parameter is strongly (Jaffe) or moderately (Hernquist) disfavored over the model with three free parameters

4. Discussion and Conclusions

Two independent methods, strong gravitational lensing and stellar dynamics, were used to determine the projected galaxy mass within its Einstein radius for a set of 58 galaxies from SLACS. From the comparison of the two masses, the lens density profile, velocity anisotropy and l.o.s. mass contamination were probed.

Even thought the maximum likelihood estimation of the l.o.s. mass contamination gives a null contribution from secondary matter along the l.o.s., the distribution of possible contamination fraction values is broad, yielding an average contamination of the order of 10%. This result is compatible with theoretical expectations coming from large-scale structure simulations (Premadi & Martel 2004; Hilbert et al. 2007; Faure et al. 2008; Puchwein & Hilbert 2009) and also with some observational works (Momcheva et al. 2006; Williams et al. 2006; Treu et al. 2008) that do find l.o.s. contamination. Auger (2008) did not find an over-density of photometric sources along the l.o.s. of a sample of SLACS strong lenses in comparison with other SDSS massive early-type galaxies. However, it is worth pointing out that this is not in contradiction with the existence of mass over-densities along the l.o.s. since SLACS

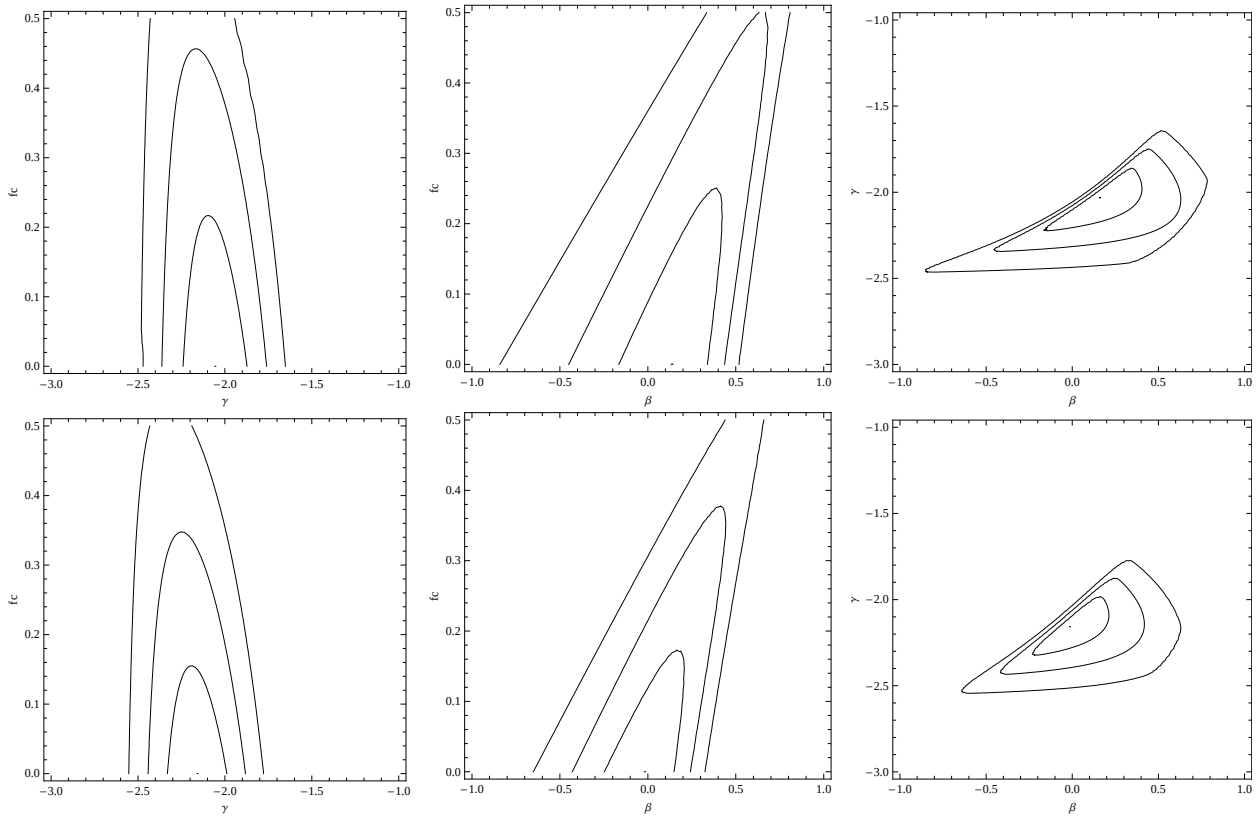

Fig. 2.— Marginalized likelihood contours, corresponding to the 1σ, 2σ and 3σ confidence levels. The parameter values of maximum marginalized likelihood are shown as points in the interior of the contours. Upper panels use Jaffe's light distribution profile and bottom panels use Hernquist's. The marginalization is over one of the three free parameters: β in the left row, γ in the center and f_c in the right.

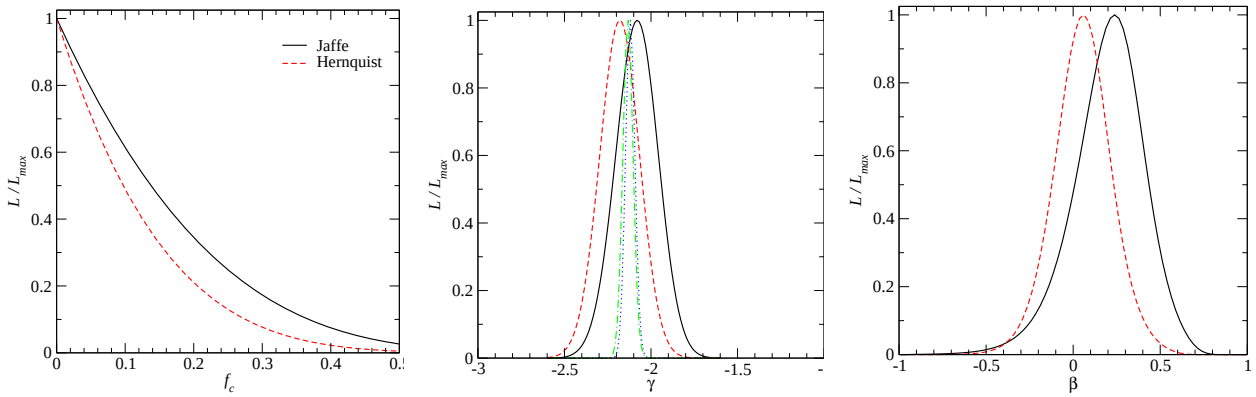

Fig. 3.— Marginalized likelihood over two parameters. The narrower curves at the center panel is for a model with fixed $f_c = \beta = 0$ and free γ, using a Hernquist luminosity density profile: the dotted line does not take into account the seeing correction and the dot-dashed line does.

Table 2: Comparison of models.

model 1: M_1	model 2: M_2	$\frac{\mathcal{L}_{max}(M_1)}{\mathcal{L}_{max}(M_2)}$	$\ln \frac{E(M_1)}{E(M_2)}$	Jeffreys' scale
J, free (f_c, γ, β)	H, free (f_c, γ, β)	14	2.9	moderate evidence for M_1
J, free (f_c, γ, β)	J, $f_c = 0$, free (γ, β)	1.0	-1.1	weak evidence for M_2
H, free (f_c, γ, β)	H, $f_c = 0$, free (γ, β)	1.0	-1.4	weak evidence for M_2
J, free (f_c, γ, β)	J, $\gamma = -2$, free (f_c, β)	1.1	-1.7	weak evidence for M_2
H, free (f_c, γ, β)	H, $\gamma = -2$, free (f_c, β)	2.4	-0.69	inconclusive
J, free (f_c, γ, β)	J, $\beta = 0$, free (f_c, γ)	1.3	-0.70	inconclusive
H, free (f_c, γ, β)	H, $\beta = 0$, free (f_c, γ)	1.0	-1.6	weak evidence for M_2
J, free (f_c, γ, β)	J, $f_c = 0$, $\gamma = -2$, $\beta = 0$	$4.6{\cdot}10^7$	11	strong evidence for M_1
H, free (f_c, γ, β)	H, $f_c = 0$, $\gamma = -2$, $\beta = 0$	$1.6{\cdot}10^4$	3.1	moderate evidence for M_1

NOTE.—J stands for Jaffe's light distribution, H for Hernquist's. Jeffreys' scale according to Trotta (2008).

lenses were selected to be isolated and excess photometric sources would only trace rare high density peaks, but not more common diffuse mass concentrations.

The shape of the $f_c \times \gamma$ and $f_c \times \beta$ degeneracies indicates that the determination of the density profile and anisotropy parameter are not very sensitive to the value of the l.o.s. contamination. This can be understood from the functional dependence of the dynamical mass with γ and β (figure 1). A small variation in γ or β implies a large change in m_D.

The joint strong lensing and stellar dynamics analysis seems to do not strongly constrain the anisotropy parameter, its likelihood distribution being broad and statistically compatible with isotropy on average. Nevertheless, the degeneracy between γ and β gives an indetermination that correlates a larger anisotropy with a flatter density profile, which can also be understood from the functional behavior of $m_D(\gamma, \beta)$ (figure 1). An increment in γ can be annulled, in terms of a variation in the dynamical mass, by a decrement in β, and vice-versa.

The inclusion of two degrees of freedom in the model with respect to the l.o.s. contamination and velocity anisotropy allows us to take into account and examine the effect of our prior ignorance on these features of the lens system. The most visible effect of f_c and β on the determination of the density profile logarithmic slope is the considerable broadening of its likelihood distribution (posterior probability), what means a more uncertain determination of γ. Within this uncertainty, the density profile is statistically compatible with an isothermal profile. This very particular density profile is also found by other authors, apparently as a result of the complementarity of baryonic and dark matter profiles (Hamana et al. 2005; Ferreras et al. 2005; Lintott et al. 2006; Baltz et al. 2007; Czoske et al. 2008).

We used standard assumptions and approximations in our modeling of galaxies and analysis. Nevertheless, we can identify several areas where further work can be done to refine the understanding of these strong lensing systems, which can also be seem as caveats to the present works in the area. Among them we highlight (i) the triaxiality and substructure of lens halos, whose importance was already suggested by Meneghetti et al. (2005) and Yencho et al. (2006) in the context of simulations on cluster scales; (ii) the correction of the dynamical mass estimate due to rotational support. It is well known that some early-type galaxies can have a significant rotational component (e.g., Emsellem et al. 2007) and two-dimensional kinematics for some few SLACS lenses are already becoming available (Czoske et al. 2008; Barnabe et al. 2009); (iii) the brightness distribution, which could be treated more realistically with the observed full surface luminosities for the individual lenses, instead of individualized fits of an universal profile; and (iv) the velocity anisotropy parameter, which was as-

sumed to be a constant, but that more realistically must be a function of radius. However very little is known about the velocity anisotropy of early-type galaxies, be it observationally, theoretically and even from simulations.

The relaxation of some of our assumptions, with the almost inevitable addition of extra free parameters, could prove a fruitful source of investigation, however would likely require a larger galaxy sample to reduce the likely increased degeneracies among the degrees of freedom of the model. As we have illustrated, models with a large number of parameters may have a higher likelihood but lower Bayesian evidence, since the added complexity must pay its price in a Bayesian sense.

The authors thank CNPq and FAPESP for financial support and the SLACS and SDSS teams for the databases used in this work.

Appendix

A.1. Solving Jean's Equation

The spherical Jeans equation (3) can be rewritten, defining $x \equiv r/R_{ef}$ (dimensionless) and

$$y \equiv \frac{3+\gamma}{4\pi GA} R_{ef}^{-(2+\gamma)} (\nu\sigma_r^2), \tag{A1}$$

as

$$\frac{dy}{dx} = -2\beta\frac{y}{x} - \nu x^{1+\gamma}. \tag{A2}$$

The luminosity distribution is well approximated by the profiles (Koopmans et al. 2006)

$$\nu(x) \propto \frac{1}{x^{\gamma_*}(x+x_*)^{4-\gamma_*}} \ , \tag{A3}$$

where $\gamma_* = 1$ and $x_* = 1/1.8153$ (Hernquist 1990), or $\gamma_* = 2$ and $x_* = 1/0.7447$ (Jaffe 1983). We examine both profiles.

The first-order linear differential equation (A2) has as solution

$$y(x) = x^{-2\beta}\left[C - \int \nu(x) x^{1+\gamma+2\beta} dx\right], \tag{A4}$$

where C is an arbitrary constant and the most evident boundary condition is $y(x \to \infty) = 0$. The analytical solution for the integral in (A4) with (A3) for $\nu(r)$ has the hypergeometric function ${}_2F_1$, which has a computationally demanding solution. Therefore we solve (A2) using a fourth order Runge Kutha algorithm, starting at $y(x = 1000) = 0$ and evolving $y(x)$ down to $x = 0.01$.

The dynamical mass (2) within the Einstein radius R_E is then

$$m_D(\gamma,\beta) = \frac{\pi^{1/2}}{2G}\frac{\Gamma\left(-\frac{1+\gamma}{2}\right)}{\Gamma\left(-\frac{\gamma}{2}\right)}\sigma_{ap}^2 R_E \left(\frac{R_E}{R_{ef}}\right)^{2+\gamma}\frac{\int_{C_E}\nu dV}{\int_{C_E} y dV}, \tag{A5}$$

and its error is estimated from the observational errors on σ_{ap} and R_E through error propagation.

A.2. Seeing

We model the effect of the seeing through a Gaussian smoothing of the galaxy projected luminosity. Therefore, the observed surface brightness profile is related to an intrinsic (no seeing) profile by

$$I_{obs}(\theta) = \frac{e^{-\theta^2/2\sigma_s^2}}{\sigma_s^2}\int_0^\infty I(\theta')\mathrm{I}_0\left(\frac{\theta\theta'}{\sigma_s^2}\right)e^{-\theta'^2/2\sigma_s^2}\theta' d\theta' \ , \tag{A6}$$

where I_0 is the modified Bessel function of first kind, and σ_s^2 is the Gaussian seeing variance. We use $\sigma_s = 0.64''$, which corresponds to a FWHM of $1.5''$.

The seeing correction of the average velocity dispersion within the observational aperture is then given by

$$\frac{\sigma_{ap}^2}{\left(\sigma_{ap}^2\right)_{obs}} = \frac{\int_0^{R_{ap}}\sigma_p^2(R)I(R)RdR}{\int_0^{R_{ap}}\left[\sigma_p^2(R)I(R)\right]_{obs}RdR}\frac{\int_0^{R_{ap}}I_{obs}(R)RdR}{\int_0^{R_{ap}}I(R)RdR} \ , \tag{A7}$$

where σ_p^2 is the projected velocity dispersion profile, $\left[\sigma_p^2(R)I(R)\right]_{obs}$ is defined in an analogous way to $I_{obs}(R)$ in Eq.(A6) and the projection is calculated through (Binney & Tremaine 1987)

$$I(R)\sigma_p^2(R) = 2\int_R^\infty\left(1-\beta\frac{R^2}{r^2}\right)\frac{\nu\sigma_r^2 r}{\sqrt{r^2-R^2}}dr. \tag{A8}$$

REFERENCES

Auger, M. W., Fassnacht, C. D., Abrahamse, A. L., Lubin, L. M., & Squires, G. K. 2007, AJ, 134, 668

Auger, M. W. 2008, MNRAS, 383, L40

Baltz, E. A., Marshall, P., & Oguri, M. 2007, ArXiv e-prints, arXiv:0705.0682

Bar-Kana, R. 1996, ApJ, 468, 17

Barnabe, M., Czoske, O., Koopmans, L., Treu, T., Bolton, A., & Gavazzi, R. 2009, arXiv:0904.3861

Binney, J. & Tremaine, S. 1987, Galactic Dynamics (Princeton: Princeton Univ. Press)

Bolton, A. S., Burles, S., Koopmans, L. V. E., Treu, T., & Moustakas, L. A. 2006, ApJ, 638, 703

Bolton, A. S., Burles, S., Treu, T., Koopmans, L. V. E., & Moustakas, L. A. 2007, ApJ, 665, L105

Bolton, A. S., Burles, S., Koopmans, L. V. E., Treu, T., Gavazzi, R., Moustakas, L. A., Wayth, R., & Schlegel, D. J. 2008, ApJ, 682, 964

Bolton, A. S., Treu, T., Koopmans, L. V. E., Gavazzi, R., Moustakas, L. A., Burles, S., Schlegel, D. J., & Wayth, R. 2008, ApJ, 684, 248

Czoske, O., Barnabè, M., Koopmans, L. V. E., Treu, T., & Bolton, A. S. 2008, MNRAS, 384, 987

Dalal, N., Hennawi, J. F., & Bode, P. 2005, ApJ, 622, 99

Emsellem, E., et al. 2007, ArXiv Astrophysics e-prints, arXiv:astro-ph/0703531

Fassnacht, C. D., Gal, R. R., Lubin, L. M., McKean, J. P., Squires, G. K., & Readhead, A. C. S. 2006, ApJ, 642, 30

Faure, C., et al. 2008, arXiv:0810.4838, ApJin press

Ferreras, I., Saha, P., & Williams, L. L. R. 2005, ApJ, 623, L5

Gavazzi, R., Treu, T., Rhodes, J. D., Koopmans, L. V. E., Bolton, A. S., Burles, S., Massey, R. J., & Moustakas, L. A. 2007, ApJ, 667, 176

Guimarães, A. C. C., & Sodré, L. J. 2007, arXiv:0706.3098

Hamana, T., Ohyama, Y., Chiba, M., & Kashikawa, N. 2005, ArXiv Astrophysics e-prints, arXiv:astro-ph/0507056

Hernquist, L. 1990, ApJ, 356, 359

Hilbert, S., White, S. D. M., Hartlap, J., & Schneider, P. 2007, MNRAS, 927

Jaffe, W. 1983, MNRAS, 202, 995

Keeton, C. R., Kochanek, C. S., & Seljak, U. 1997, ApJ, 482, 604

Koopmans, L. V. E., Treu, T., Bolton, A. S., Burles, S., & Moustakas, L. A. 2006, ApJ, 649, 599

Koopmans, L. V. E., et al. 2009, ApJ, 703, L51

Lintott, C. J., Ferreras, I., & Lahav, O. 2006, ApJ, 648, 826

Meneghetti, M., Bartelmann, M., Jenkins, A., & Frenk, C. 2005, ArXiv Astrophysics e-prints, arXiv:astro-ph/0509323

Meylan, G., Jetzer, P., North, P., Schneider, P., Kochanek, C. S., & Wambsganss, J. 2006, Saas-Fee Advanced Course 33: Gravitational Lensing: Strong, Weak and Micro

Momcheva, I., Williams, K., Keeton, C., & Zabludoff, A. 2006, ApJ, 641, 169

Moustakas, L. A., et al. 2007, ApJ, 660, L31

Premadi, P., & Martel, H. 2004, ApJ, 611, 1

Puchwein, E., & Hilbert, S. 2009, arXiv:0904.0253

Tonry, J. L., & Kochanek, C. S. 2000, AJ, 119, 1078

Treu, T., Koopmans, L. V., Bolton, A. S., Burles, S., & Moustakas, L. A. 2006, ApJ, 640, 662

Treu, T., Gavazzi, R., Gorecki, A., Marshall, P. J., Koopmans, L. V. E., Bolton, A. S., Moustakas, L. A., & Burles, S. 2008, arXiv:0806.1056

Trotta, R. 2008, Contemporary Physics, 49, 71

Yencho, B. M., Johnston, K. V., Bullock, J. S., & Rhode, K. L. 2006, ApJ, 643, 154

Wambsganss, J., Bode, P., & Ostriker, J. P. 2005, ApJ, 635, L1

Williams, K. A., Momcheva, I., Keeton, C. R., Zabludoff, A. I., & Lehár, J. 2006, ApJ, 646, 85

This 2-column preprint was prepared with the AAS LaTeX macros v5.2.